Biochimica et Biophysica Acta 1848 (2015) 967–975

Contents lists available at ScienceDirect

Biochimica et Biophysica Acta

journal homepage: www.elsevier.com/locate/bbamem

Partially induced transition from horizontal to vertical orientation of helical peptides at the air–water interface and the structure of their monolayers transferred on the solid substrates

Noritaka Kato [a,b,*], Takanori Sasaki [a,c], Yuri Mukai [a,b]

[a] Graduate School of Science and Engineering, Meiji University, Kawasaki 214-8571, Japan
[b] School of Science and Engineering, Meiji University, Kawasaki 214-8571, Japan
[c] School of Interdisciplinary Mathematical Sciences, Meiji University, Tokyo 164-8525, Japan

ARTICLE INFO

Article history:
Received 6 August 2014
Received in revised form 18 December 2014
Accepted 24 December 2014
Available online 3 January 2015

Keywords:
Amphiphilic peptide
α-Helix
Air–water interface
Langmuir–Blodgett film

ABSTRACT

To apply the Langmuir–Blodgett (LB) technique as a platform for investigating the fundamental properties of amphiphilic peptides (APs), we have investigated the structure of LB films using the APs. To vertically orient the helical APs like transmembrane proteins in the membrane, the primary structure of the APs was designed to have two domains: a hydrophilic domain (three amino acids) and a hydrophobic domain (ca. 20 amino acids). However, we are still far from having full control of their orientation. This study reports the contribution of the subphase temperature to the change in the orientation of helical APs. When the surface pressure–area isotherm of AP was observed at the subphase temperature at 41.5 °C, the isotherm exhibited a plateau, implying that a phase transition of the monolayer at the air–water interface occurred. Circular dichroism (CD) spectra of the monolayers transferred on the solid substrates revealed that the orientation of the helices changed at the pressure, where the plateau of the isotherm was observed. This change was not observed at 21.5 °C, i.e., the horizontal alignment of helixes was maintained. Atomic force microscopy (AFM) was used to systematically investigate the surface structure of the monolayers transferred at different surface pressures. A structural model of the monolayer that did not contradict with the results obtained by the three different techniques (the isotherm, CD spectroscopy, and AFM) was derived, and it was concluded that the horizontally oriented helices partially changed their orientation to vertical upon compression in the plateau region of the isotherm.

1. Introduction

Because of their amphiphilic nature, membrane proteins are more difficult to investigate than water-soluble proteins [1]. To isolate them from cells, a treatment using detergents is required. To investigate their biological functionality, they have to be placed in similar conditions as in the cell, e.g., reconstitution of membrane proteins into lipid vesicles. Because of these obstacles, the progress in the structure determination of membrane proteins is far behind water-soluble proteins [2], even though one-third of proteins encoded in the human genome are membrane proteins [3,4] and more than half of pharmaceutical targets correspond to membrane proteins [5,6]. Therefore, tremendous efforts are being made to understand the chemical and biological functionalities and the structure of membrane proteins, as well as to develop techniques for their characterization [7,8]. Besides the direct investigation of the proteins themselves, there is a "divide and conquer" approach to membrane proteins [9–11]. In this approach, fragments of the membrane proteins (peptides) are the targets investigated to understand the membrane proteins. When the protein is disassembled into peptides, the above-mentioned difficulties in the membrane proteins are reduced and various experimental techniques can be applied. Specifically, in the case of α-helical peptides, which correspond to one of the transmembrane (TM) domains of the α-helical TM proteins, the experimental techniques and the TM domains investigated have been summarized in Ref. [11]. However, the application of the Langmuir–Blodgett (LB) technique to TM peptides was hardly mentioned.

The LB technique, which involves studying the monolayer at the gas–liquid interface (Langmuir monolayer), has been applied to various peptides to understand the fundamental properties of polypeptides [12] and develop molecular architectures [13–15]. However, in the case of helical peptides, it is difficult to align the helical axis perpendicular to the interface [13,14,16–24], and vertically oriented helical peptides often contain non-gene encoded amino acids (AAs) [14,16,17,19,21–23]. This is one of the reasons why the LB technique is rarely applied to investigate the TM peptides in biological aspects. To use the LB technique as a platform to investigate the fundamental properties of TM peptides, how the helical axis of peptides consisting of the gene-

* Corresponding author at: Graduate School of Science and Engineering, Meiji University, Kawasaki 214-8571, Japan. Tel./fax: +81 44 934 7292.
E-mail address: nkato@meiji.ac.jp (N. Kato).

http://dx.doi.org/10.1016/j.bbamem.2014.12.022
0005-2736/

encoded AAs can be oriented perpendicular by the LB technique needs to be studied, because the TM domains of the TM proteins vertically orient to the cell membrane.

Gas–liquid and gas–solid interfaces are unfavorable situations for mimicking the membrane environment of TM peptides. Conversely, because of the advantage of the LB technique, we could apply a variety of spectroscopic and microscopic methods that are surface- and interface-sensitive to analyze and determine the structure and dynamics of materials at the interface [20,25–35]. This will help to understand the fundamental properties of TM peptides.

Thus, we restricted ourselves to peptides whose AAs are gene-encoded and whose sequences consist of hydrophobic and hydrophilic domains [36,37]. Because of the two domains, when the peptides form the α-helical conformation, amphiphilic helices are formed, and they are expected to orient their helical axes perpendicular to the surface of the aqueous subphase. Recently, we had indicated that amphiphilic peptides (APs) whose AA sequences of the hydrophobic domains are the same as TM peptides proposed for the lipid bilayer [38,39] are able to form an α-helix at the air–water interface and these helices partially orient perpendicular in peptide/lipid mixed LB films [37].

The present work aims to further investigate the important parameters that determine the orientation of the amphiphilic helices at the air–water interface, and we have investigated how the temperature at the air–water interface and the hydrophobic moment (HM) of the hydrophobic domain of the peptide affect the controllability of the orientation of the amphiphilic helices by the LB technique. For simplicity, the Langmuir monolayers of the APs were formed without lipids, and the AA sequences of the APs for the monolayers are shown in Table 1. K3-19W is one of the peptides we have used previously [37]. To investigate the influence of the HM value on the orientation of the helical AP in the monolayers, the W residue of K3-19W was changed to the A residue to reduce the HM value of the hydrophobic domain. This AP was called K3-19A. The helical wheel projections of their hydrophobic domains are shown in Fig. 1 together with the values and the directions of the HMs. The HM values were calculated using the equation in Ref. [40] and the hydrophobicity values used for the calculation were the whole-residue hydrophobicity scale for the lipid bilayer interface (ΔG_{wif}) [41]. The temperature dependence of the surface pressure–area (π–A) isotherm of the Langmuir monolayer of AP was investigated. The circular dichroism (CD) spectra of the Langmuir monolayers transferred on the solid substrates by the LB technique (1-layer LB films) were recorded to analyze the orientation of the helices. The topography images of the 1-layer LB films of the APs were obtained by atomic force microscope (AFM). A structure model of the 1-layer LB film that does not contradict with the results obtained by three different techniques was deduced.

2. Experimental

The APs consisting of 22 AAs (Table 1) were synthesized by Operon Biotechnologies, K.K. (Tokyo, Japan) and their purities were >90%. Pure water (>18 MΩ cm) was prepared in a Milli-Q system (Elix Advantage 3, Merck Millipore, Darmstadt, Germany). All of the organic solvents, citric acid, and trisodium citrate were purchased from Wako Pure Chemical Industries Ltd. (Osaka, Japan).

Table 1
Primary structure and average hydrophobicity scale [41] of the amphiphilic peptides.

Abbreviation	Primary structure	Average hydrophobicity scale[a]
K3-19W	NH_2–KKKALALAAAALWLAAAALALA–$CONH_2$	−0.009 kcal/mol
K3-19A	NH_2–KKKALALAAAALALAAAALALA–$CONH_2$	0.083 kcal/mol

The underlined parts correspond to the hydrophobic domains.
[a] Because the hydrophobic/hydrophilic residues are scaled to be negative/positive, the average scale indicates that K3-19A has lower hydrophobicity than K3-19W.

The solvent for the spreading solution of the APs was dichloromethane/methanol (5:2 v/v), and the concentrations of K3-19W and K3-19A in the spreading solutions were 47.2 and 49.9 μM, respectively. A citric acid–sodium citrate buffer (5 mM, pH 6.0) was used for the aqueous subphase of the Langmuir monolayer, and the temperature of the subphase was controlled at 21.5 ± 0.5, 31.5 ± 0.5, or 41.5 ± 0.5 °C. At pH 6.0, the three K residues are expected to be protonated.

The π–A isotherms of the Langmuir monolayer were measured by the trough with two movable barriers (MiniMicro LB system, KSV NIMA, Biolin Scientific Holding AB, Stockholm, Sweden). The inner width (effective barrier width) and the inner length of the trough were 50 and 170 mm, respectively. The spreading solution was spread drop by drop on the subphase by a micro syringe. A period of 10 min was allowed for the solvent evaporation before compression of the Langmuir monolayer, and the compression speed was 500 mm^2/min. The number of molecules spread on the subphase for a single measurement of the isotherm was 1.14×10^{15} and 0.90×10^{15} for K3-19W and K3-19A, respectively, corresponding to 40 and 30 μL of the spreading solution of K3-19W and K3-19A, respectively.

For the CD measurements, the Langmuir monolayer on the subphase was transferred at specific surface pressures (π_{dep}'s) to the fused silica substrate (10 mm × 40 mm) by the vertical deposition method [42]. The CD spectra were recorded using a J-820 CD spectropolarimeter (JASCO Corp., Tokyo, Japan), and the temperature of the 1-layer LB films was kept at 20 °C during the measurements by the sample holder equipped with the thermoelectric (Peltier) devices. The 1-layer LB film was set perpendicular to the optical axis of the spectropolarimeter. An elementary analysis of the helix orientation was performed on the CD spectra under the assumption that all of the APs in the 1-layer LB film formed an α-helix [37]. The shape of the CD spectrum depends on the angle between the incident axis and the helical axis of the α-helix. The spectral shapes as a function of wavelength when the incident axis is parallel to the helical axis ($G_1(\lambda)$) and when the incident axis is perpendicular to the helical axis ($G_2(\lambda)$) are given in Ref. [43]. When the helices are uniformly oriented at a tilt angle (θ) of the helical axis from the film normal, the CD spectrum of the 1-layer LB film, whose plane is perpendicular to the optical axis of the spectropolarimeter, is given by

$$\mathrm{CD}(\lambda, \theta) = C\left\{G_1(\lambda)\cos^2\theta + G_2(\lambda)\sin^2\theta\right\}, \quad (1)$$

where C is the amplitude coefficient.

The surface morphology of the 1-layer LB film was observed by AFM (Dimension Icon, Bruker AXS GmbH, Karlsruhe, Germany) in tapping mode. The Langmuir monolayer of the AP was deposited on a fleshly cleaved mica substrate (8 mm × 51 mm) by the vertical deposition method [42] at a given π_{dep}. The resonant frequency and the spring constant of the cantilever (NCHV-10 V) were 361–400 kHz and 20–80 N/m, respectively. The topography image was collected at 512 × 512 pixel resolution. The flattening of the obtained images and the analyses of the height histogram were carried out using the software WSxM [44].

For the vertical deposition of the Langmuir monolayer, the trough with two movable barriers was used except for the deposition of the monolayer of K3-19W at π_{dep} = 29 mN/m from the subphase at 41.5 °C. In this condition, the trough with a single movable barrier (Filgen, Inc., Nagoya, Japan) had to be used because the barrier can move in a wider range and this trough can compress the Langmuir monolayer into a smaller area than the trough with two barriers. The inner width and length of this trough were 80 and 525 mm, respectively, and the compression speed was 880 mm^2/min. The Langmuir monolayer was compressed up to π_{dep} and was stabilized for 5–15 min before the deposition. During the deposition, the substrate was vertically lifted from the subphase to air at 6 mm/min for both troughs, and the surface pressure was kept constant at π_{dep}. The transfer ratio, which is defined as the decrease in area of the Langmuir monolayer during the deposition divided

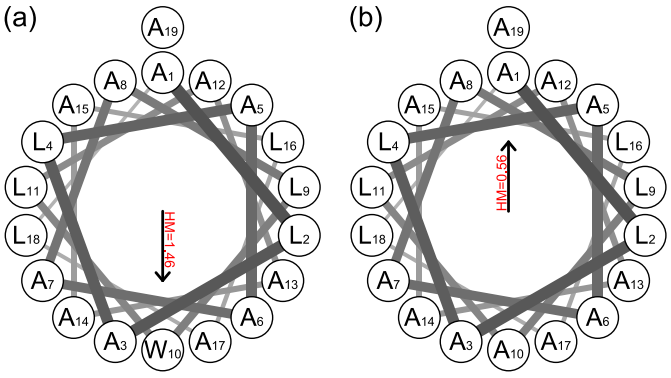

Fig. 1. Helical wheel projections of (a) K3-19W and (b) K3-19A. The value and arrow indicate the value and direction of hydrophobic moment (HM).

by the area of the substrate moved across the air–water interface during the deposition, was 1 ± 0.15 under all conditions, unless specified otherwise.

3. Results and discussion

3.1. π–A isotherm

The *π–A* isotherms of K3-19W at three different subphase temperatures are shown in Fig. 2a. In all cases, the limiting molecular areas estimated by extrapolating the isotherm from ca. 23 to 0 mN/m ranged from 3 to 4 nm^2/molecule. The helix can be treated as a cylinder, and the radius and length of the cylinder per AA residue are expected to be 0.5–0.55 and 0.15 nm, respectively [13,21]. Thus, when the helix of 22 AAs lies horizontally to the interface, the molecular area is expected to be 3.3–3.63 nm^2/helix. Therefore, up to 23 mN/m, the horizontally oriented helices were compressed. The isotherm obtained at 21.5 °C (Fig. 2a) exhibited a kink at ca. 25 mN/m. Above this pressure, the isotherm went wavy, suggesting that the collapse pressure of the monolayer at 21.5 °C was around 25 mN/m. The isotherm obtained at 31.5 °C (Fig. 2a) also exhibited a kink at 25 mN/m but showed a plateau-like region from 2.5 to 1.5 nm^2/molecule. A further increase in the subphase temperature (41.5 °C) made the plateau region of the isotherm clearer (at 24 mN/m, Fig. 2a). In addition, below 1 nm^2/molecule, the isotherm exhibited a steep increase, implying that the phase transition accompanying the change in the helix orientation occurred at the plateau. In the case of K3-19A, the isotherm at 41.5 °C (Fig. 2b) also exhibited a plateau 4 mN/m lower than that observed for K3-19W.

3.2. CD spectra

The CD spectra of the 1-layer LB films were analyzed using Eq. (1) assuming that all the helices oriented at a uniform angle θ. The 1-layer LB film of K3-19W deposited from the subphase at 21.5 °C showed $\theta = 90°$ irrespective to the surface pressure. Fig. 3a and b show the spectra of the 1-layer LB films prepared at $\pi_{dep} = 6.5$ and 30 mN/m, respectively. At $\pi_{dep} = 30$ mN/m, the average transfer ratio was 0.63. This low transfer ratio can be attributed to the deposition pressure being higher than the collapse pressure of the Langmuir monolayer (ca. 25 mN/m, Fig. 2a, thick blue line). The spectra are fitted well by $\theta = 90°$. Therefore, on the subphase at 21.5 °C, the helices of K3-19W orient horizontally to the surface at any surface pressure. This result indicates that the hydrophobic surface of the helix has to contact with the aqueous subphase. Because the α-helix has aligned electric dipole moments along the helical axis from the C- to N-terminus [45], the dipole–dipole interaction between the helices may form aggregates of helices aligned in an anti-parallel manner (Fig. 3c) [46]. Because of the anti-parallel alignment of the amphiphilic helices, the hydrophilic domains are at both sides of the aggregate and may stabilize the contact of the hydrophobic surface of the helix with the aqueous subphase. By keeping the helical axis parallel to the subphase, these helices and/or aggregates were compressed and overlapped with each other above 25 mN/m, because the molecular area at 30 mN/m (1.53 nm^2/molecule, Fig. 2a, thick blue line) is smaller than the expected molecular area of the helix horizontally oriented on the subphase (3.3–3.63 nm^2/helix).

At a subphase temperature of 41.5 °C, the CD spectra of the 1-layer LB films of K3-19W depended on the surface pressure (Fig. 4). Up to $\pi_{dep} = 22$ mN/m, $\theta = 90°$ (Fig. 4a and b). At $\pi_{dep} = 24$ mN/m, where the plateau of the isotherm was observed (Fig. 2a, thin black line), θ decreased to 66° (Fig. 4c). At $\pi_{dep} = 26$ mN/m, where the steep increase in the isotherm after the plateau was observed, a further decrease in θ to 52° was observed (Fig. 4d). θ then slightly decreased to 49° at $\pi_{dep} = 29$ mN/m. These results indicate that the orientation of the helices changed at the surface pressure where the plateau of the isotherm was observed. With the increase in the subphase temperature from 21.5 to 41.5 °C, the increased thermal fluctuation broke up the aggregates formed by dipole–dipole interactions (Fig. 3c) and the helices decreased the tilt angle (θ) upon compression to reduce the contact between the hydrophobic surface of helix and the aqueous subphase.

As with K3-19W, the 1-layer LB film of K3-19A deposited from the subphase at 41.5 °C also showed a dependence of θ on the surface pressure. At the surface pressure where the plateau of the isotherm was observed (ca. 20 mN/m, Fig. 2b, thick green line), a decrease in θ

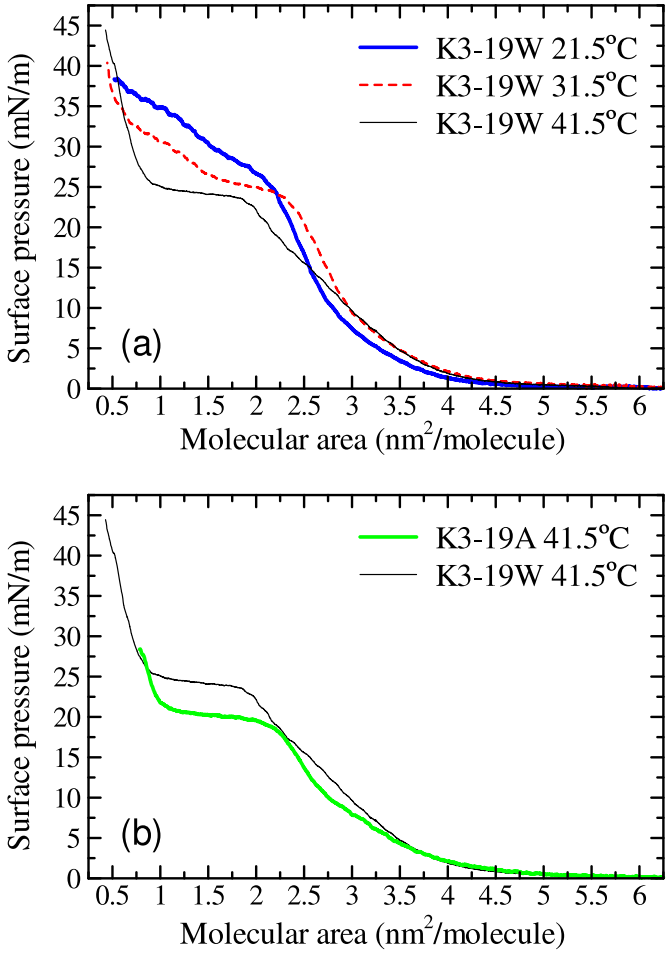

Fig. 2. (a) *π–A* isotherms of K3-19W at 21.5 ± 0.5 (thick blue line), 31.5 ± 0.5 (dashed red line), and 41.5 ± 0.5 °C (thin black line). (b) *π–A* isotherms of K3-19W (thin black line) and K3-19A (thick green line) at 41.5 ± 0.5 °C. The isotherms were reproduced at least three times.

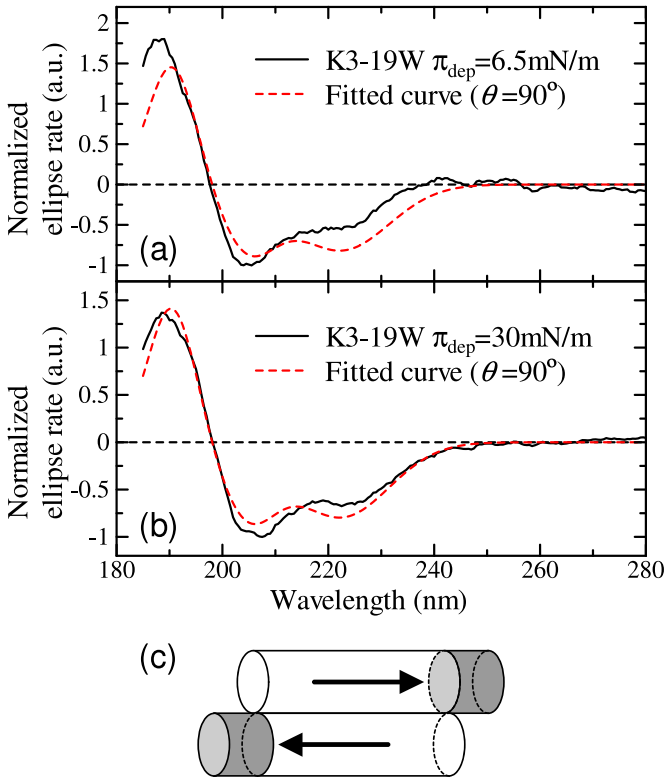

Fig. 3. Normalized CD spectra of the 1-layer LB films of K3-19W deposited from the subphase at 21.5 °C (solid black line), and the fitted curve using Eq. (1) (dashed red line). The negative peak was normalized at −1. (a) π_{dep} = 6.5 mN/m. (b) π_{dep} = 30 mN/m. (c) Anti-parallel alignment of amphiphilic helices. The white and gray faces correspond to the hydrophobic and hydrophilic surfaces, respectively.

from 90° to 55° was observed. The CD spectra and their fitted curves are shown in Fig. S2 in the Supplementary Information (SI). The shapes of the CD spectra of the 1-layer LB films of K3-19A correspond well to those of the 1-layer LB films of K3-19W. When θ = 90°, the spectral shapes shown in Fig. S2a and b for K3-19A and Fig. 4a and b for K3-9W are the same. The spectrum at θ = 55° for K3-19A (Fig. S2c) is almost identical to that at θ = 52° for K3-19W (Fig. 4d). Thus, the helical structures of K3-19A and K3-19W were the same. The relationships between θ and surface pressure for K3-19W and K3-19A are shown in Fig. 5.

3.3. AFM observation

The surface morphology of the 1-layer LB film was observed using AFM. The 1-layer LB film of K3-19W deposited from the subphase at 21.5 °C exhibited a very flat surface at π_{dep} = 6.5 mN/m (Fig. 6a). At 6.5 mN/m, the molecular area was 3.1 nm^2/molecule (Fig. 2a, thick blue line), which is close to the area expected for a horizontally oriented helix consisting of 22 AAs (3.3–3.63 nm^2/helix). The molecular area and the analysis of the CD spectrum showing that the helices oriented horizontally (Fig. 3a) indicate that the horizontally oriented helices compactly covered the surface of the substrate without overlapping. At π_{dep} = 30 mN/m, where the transfer ratio was 0.63, the surface of the 1-layer LB film was not as smooth as that deposited at 6.5 mN/m, and showed stripe patterns that were 1–7 nm higher than the average surface height (Fig. 6b). The profile of the section in Fig. 6b is shown in Fig. S3 in the SI. Although the CD analysis indicated that the helices oriented horizontally (Fig. 3b), the molecular area at 30 mN/m (Fig. 2a, thick blue line) was smaller than that expected for horizontally oriented helices, indicating that these protruding stripes are regions where the helices overlapped. Therefore, the overlapping of helices occurred inhomogeneously upon compression, and this overlap was mechanically induced by the barriers, because the strip patterns appeared almost perpendicular to the direction where the barriers of the trough moved.

The AFM images of the 1-layer LB films of K3-19W deposited at π_{dep} = 10 and 22 mN/m from the subphase at 41.5 °C are shown in Fig. 7. Even at surface pressures lower than 24 mN/m, where the plateau

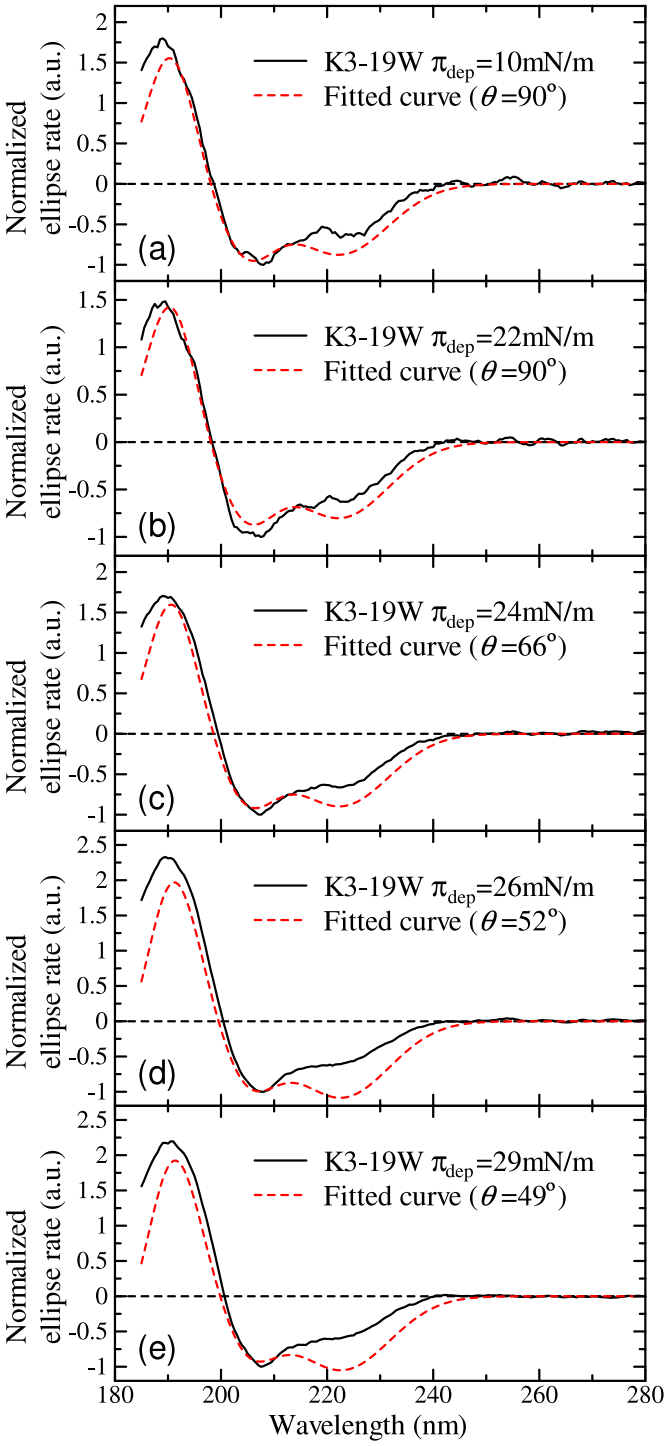

Fig. 4. Normalized CD spectra of the 1-layer LB film of K3-19W deposited from the subphase at 41.5 °C (solid black line) and the fitted curve using Eq. (1) (dashed red line). The negative peak was normalized at −1. (a) π_{dep} = 10 mN/m. (b) π_{dep} = 22 mN/m. (c) π_{dep} = 24 mN/m. (d) π_{dep} = 26 mN/m. (e) π_{dep} = 29 mN/m. The raw CD spectra are shown in Fig. S1 in the Supplementary Information.

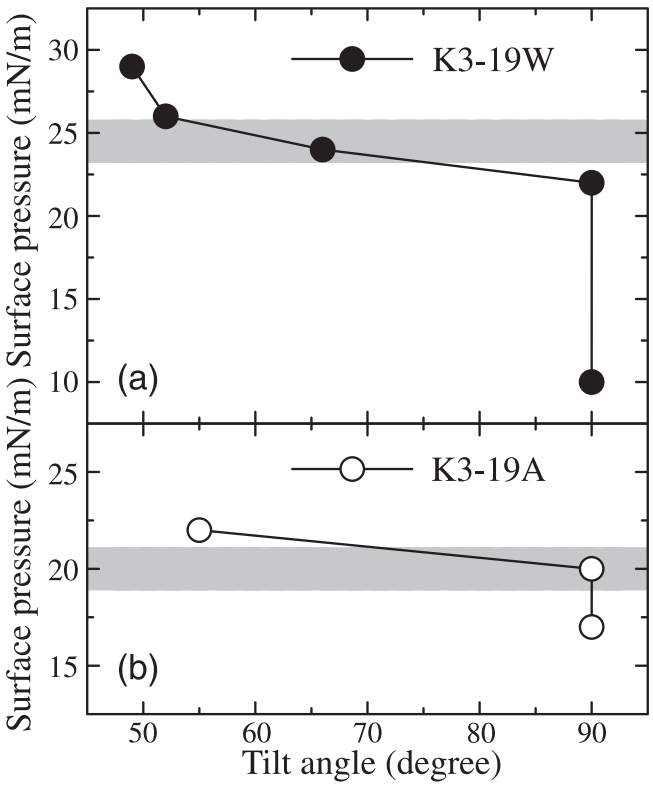

Fig. 5. Relationship between the tilt angle (θ) and the surface pressure (π_{dep}) of (a) K3-19W and (b) K3-19A. The tilt angles of the helical axis (θ) from the film normal were determined from the CD spectra. The horizontal thick gray line shows the surface pressure where the plateau of the isotherm was observed.

of the isotherm was observed, the surface of the 1-layer LB film was not as smooth as expected, and protruding stripes similar to Fig. 6b were observed. The height of the stripes ranged from 1 to 4 nm. The section profiles of the images in Fig. 7 are shown in Figs. S4 and S5 in the SI. When the two images in Fig. 7 are compared, the number of stripes increases with increasing surface pressure. Since the CD analysis in Fig. 4a and b indicated that the helices were horizontally oriented up to 22 mN/m, the protruding stripes can be ascribed to the regions where the helices overlapped, as in Fig. 6b.

When the 1-layer LB film of K3-19W was deposited at 24 mN/m from the subphase at 41.5 °C, the morphology changed. Because the deposition pressure (24 mN/m) was in the plateau region in the isotherm, the pattern of the images was not well-reproduced. The images of extreme cases are shown in Fig. 8a and b. The images observed at π_{dep} = 24 mN/m often consisted of patterns of these two images. Thus, the surface morphology dramatically changed as the helix orientation changed at around 24 mN/m (Fig. 5a). The images consisted of two different height regions. The average height difference between the two regions (Δd) and the area ratio between the high and low regions (A_H:A_L) of the image in Fig. 8b were determined to be 0.9 nm and 52:48, respectively, from analysis of the height histogram shown in Fig. S6 in the SI. According to the uniformly oriented model in Eq. (1) used for the analysis of the CD spectra, the film surface was expected to be flat and smooth. However, the two different height regions in the AFM images with ca. 1 nm height difference clearly indicated that the orientation of the helices in the 1-layer LB film was not uniform.

Further increase of π_{dep} reduced the area of the low height regions (Fig. 9) with A_H:A_L = 69:31 at π_{dep} = 26 mN/m and A_H:A_L = 77:23 at 29 mN/m. The analyses of the height histogram are shown in Fig. S7 in the SI. Upon compression, the high domains in Fig. 8b at π_{dep} = 24 mN/m merged and grew larger, resulting in the high height regions in Fig. 9a at π_{dep} = 26 mN/m. Since the isotherm showed low compressibility above 26 mN/m (Fig. 2a, thin black line), the pattern showed few changes upon compression from 26 to 29 mN/m (Fig. 9). The Δd value also did not significantly change (0.64 and 0.81 nm at π_{dep} = 26 and 29 mN/m, respectively). According to the uniform-orientation analysis of the CD spectra, all of the helices are expected to orient at θ = 52° and 49° at π_{dep} = 26 and 29 mN/m, respectively (Fig. 5a), and the surface of the 1-layer LB film should be flat. However, the surface consisted of a lot of trenches with 0.5–1 nm depth (Fig. 9). Thus, the uniform-orientation model cannot be applied even above the surface pressure where the plateau of the isotherm was observed.

The surface morphology of the 1-layer LB film of K3-19A prepared from the subphase at 41.5 °C (Fig. 10) also exhibited a similar trend to that observed in the case of K3-19W. Below the plateau of the isotherm at around 20 mN/m (Fig. 2b, thick green line), the pattern of the protruding stripes with height from 1 to 2 nm was observed at 17 mN/m (Fig. 10a, see Fig. S8 in the SI for the section analysis), and their direction was predominantly oriented perpendicular to the direction that the barriers moved, as observed in Fig. 7. At π_{dep} = 20 mN/m, corresponding to the plateau region in the isotherm (Fig. 2b, thick green line), the morphology greatly changed: the stripes disappeared and the regions ca. 1.5 nm higher than surroundings appeared (Fig. 10b, see Fig. S9 in the SI for the section analysis). The orientation of the helices in the 1-layer LB film was horizontal up to 20 mN/m (Fig. 5b). The protruding

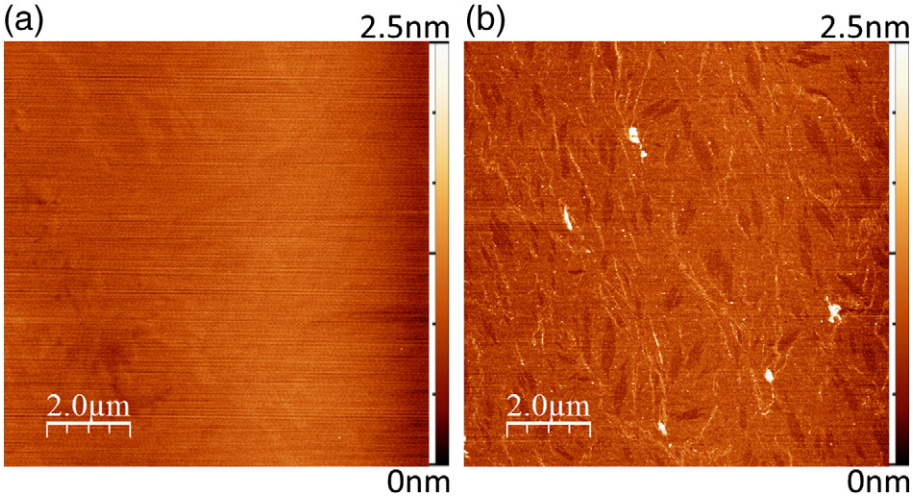

Fig. 6. AFM images of the 1-layer LB films of K3-19W deposited to the mica substrate from the subphase at 21.5 °C. (a) π_{dep} = 6.5 mN/m. (b) π_{dep} = 30 mN/m.

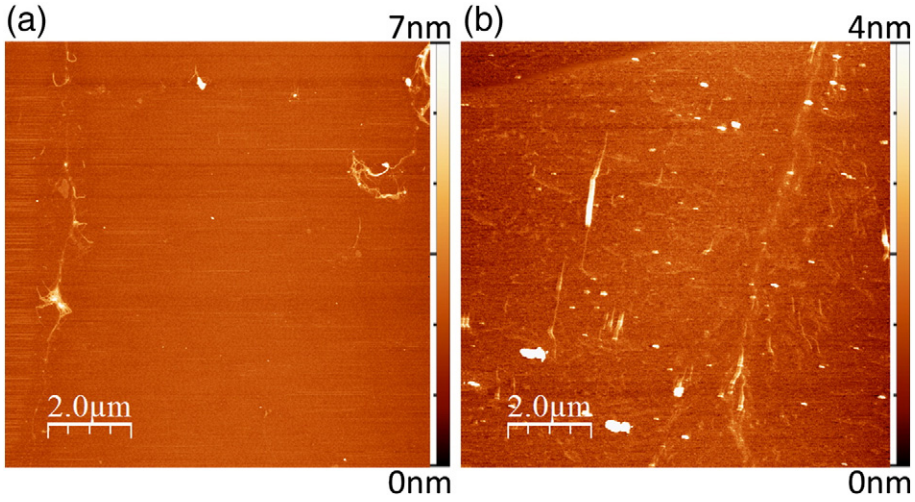

Fig. 7. AFM images of the 1-layer LB films K3-19W deposited on the mica substrate from the subphase at 41.5 °C. (a) $\pi_{dep} = 10$ mN/m. (b) $\pi_{dep} = 22$ mN/m.

stripes observed at $\pi_{dep} = 17$ mN/m and the domains 1.5 nm higher than the surrounding layer observed at $\pi_{dep} = 20$ mN/m formed by the overlap of helices with an anti-parallel alignment, as shown in Fig. 3c.

At 22 mN/m, which is slightly above the surface pressure of the plateau in the isotherm, the area of the high regions increased (Fig. 10c) together with a change in the tilt angle from 90° to 55° (Fig. 5b). According to a height histogram analysis of Fig. 10c (see

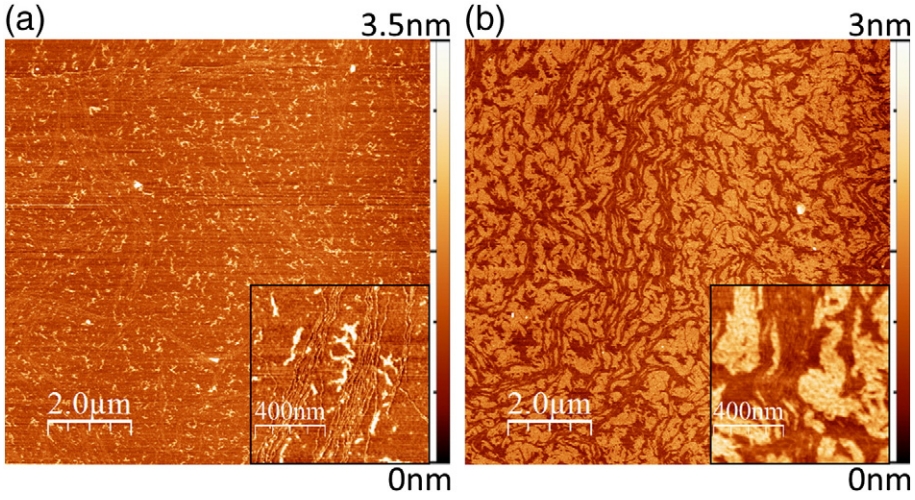

Fig. 8. AFM images of the 1-layer LB films of K3-19W deposited on the mica substrate at $\pi_{dep} = 24$ mN/m from the subphase at 41.5 °C. The insets are magnified images.

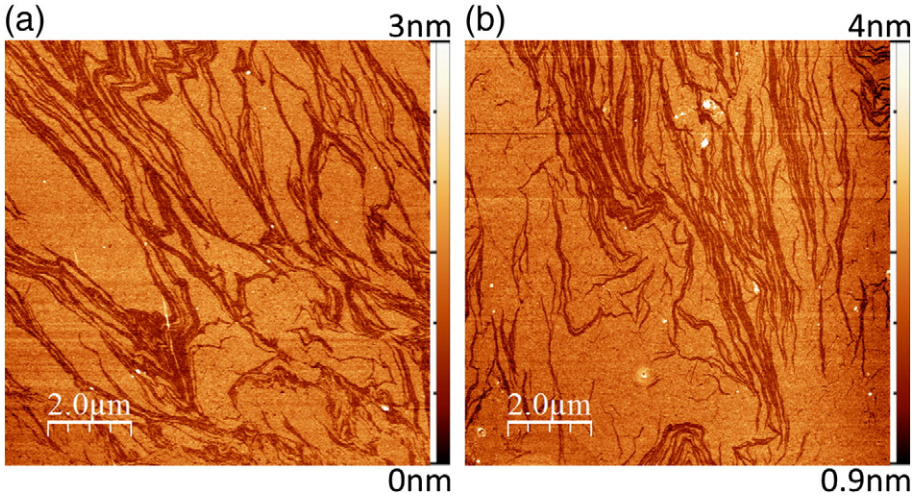

Fig. 9. AFM images of the 1-layer LB films of K3-19W deposited on the mica substrate from the subphase at 41.5 °C. (a) $\pi_{dep} = 26$ mN/m. (b) $\pi_{dep} = 29$ mN/m.

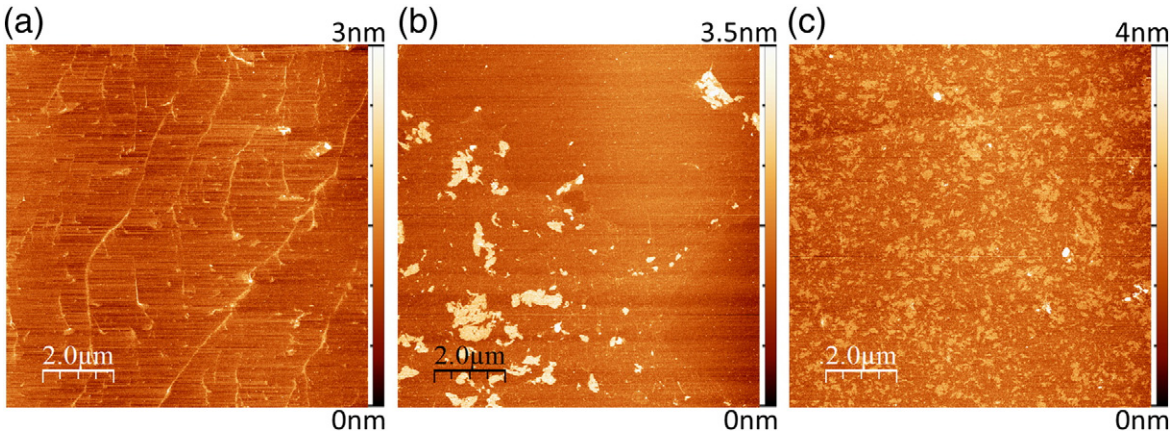

Fig. 10. AFM images of the 1-layer LB films of K3-19A deposited on the mica substrate from the subphase at 41.5 °C. (a) π_{dep} = 17 mN/m. (b) π_{dep} = 20 mN/m. (c) π_{dep} = 22 mN/m.

Fig. S10 in the SI for the histogram), the area ratio between the high and low regions (A_H:A_L) is 24:76 and the average height difference (Δd) is 0.64 nm. Thus, in the case of the 1-layer LB film of K3-19A deposited at 22 mN/m from the subphase at 41.5 °C, the uniform-orientation model also cannot be applied.

3.4. Structure model for the monolayer with $\theta < 90°$

Because the uniform orientation model in Eq. (1) is not suitable for the monolayer with $\theta < 90°$, an alternative model is required. At surface pressures lower than that at the plateau in the isotherm observed for the subphase temperature of 41.5 °C, overlap of the horizontally oriented helices was observed in the AFM images (Figs. 7a, b, and 10a). The overlap occurred inhomogeneously and striped patterns or domains were formed. The formation of these stripes and domains consisting of bundles of anti-parallel helices (Fig. 3c) corresponded to the nucleation and growth of aggregates of helices, whose growth direction was oriented not only in the in-plane but also in the out-of-plane direction of the interface, i.e., a 3-dimensional (3D) growth mode. This 3D growth mode was induced by compression of the Langmuir monolayer even at a surface pressure lower than that at the plateau of the isotherm and is the dominant growth mode in the Langmuir monolayer at the subphase temperature of 21.5 °C (Fig. 6a and b). To explain the changes in the CD spectra observed at a surface pressure higher than that at the plateau in the isotherm, we have to introduce another mode for the change in the molecular arrangement upon compression: the mode of transformation in the tilt angle of the helices from $\theta = 90°$ to $\theta < 90°$ without overlap. Thus, we assumed that the two modes (3D growth mode, where the helical axes were maintained at $\theta = 90°$, and transformation mode from $\theta = 90°$ to $\theta < 90°$) progressed upon compression of the Langmuir monolayer. It is also suspected that these two modes cannot occur in the same region of the Langmuir monolayer. Therefore, it is assumed that the growth of the two modes simultaneously occurred at the different regions of the Langmuir monolayer and formed two different height regions, as observed in Figs. 8b, 9a, b, and 10c. Therefore, the plateaus of the isotherms do not correspond to a real phase transition like the liquid–solid phase transition in the Langmuir monolayers of lipids [47].

Under these assumptions, we can deduce the structure of the Langmuir monolayer, as shown in Fig. 11. $N_{90°}$ is the number of overlapping helices in the domain induced by the 3D growth mode, and their helical axes are parallel to the interface ($\theta = 90°$). N_θ is the number of helices with a tilt angle $\theta < 90°$, and the region of non-overlapping N_θ helices is induced by the transformation mode. The three unknown values ($N_{90°}$, N_θ, and θ) were determined using the equations of the three measureable values (Eqs. 2–4), the height difference (Δd) obtained by the height histogram analyses of the AFM images (Figs. S6, S7a and b, and S10 in the SI), the area ratio between the high and low regions (A_H:A_L) of the AFM images (Figs. S6, S7a, b, and S10), and the molecular area (MA) obtained from the isotherm (Fig. 2b).

When the shape of the α-helix is treated as a cylinder, the radius (r) and the length of the cylinder per AA residue are expected to be 0.5–0.55 and 0.15 nm, respectively [13,21], as mentioned above. The length of the helix is 0.15 × 22 = 3.3 nm. Therefore, the values of Δd (nm), A_H:A_L, and MA (nm^2/molecule) are given by following equations:

$$\Delta d = \left|\left\{2r + (N_{90°} - 1)\sqrt{3}r\right\} - 3.3\cos\theta\right|, \tag{2}$$

$$A_H : A_L = 3.3r : \frac{\pi r^2}{\cos\theta}N_\theta \quad \text{or} \quad \frac{\pi r^2}{\cos\theta}N_\theta : 3.3r, \tag{3}$$

$$\mathrm{MA} = \frac{2r \times 3.3 + \dfrac{\pi r^2}{\cos\theta}N_\theta}{N_{90°} + N_\theta}. \tag{4}$$

Using the calculated values of $N_{90°}$, N_θ, and θ, the CD spectrum was reproduced by the following equation:

$$\mathrm{CD}_{\mathrm{Rep}}(\lambda,\ \theta) = C'\left[N_\theta\left\{G_1(\lambda)\cos^2\theta + G_2(\lambda)\sin^2\theta\right\} + N_{90°}G_2(\lambda)\right], \tag{5}$$

where C' is a constant, and the root mean square (RMS) of the difference between the calculated and measured spectra was evaluated. The use of r = 0.5 or 0.55 in(3) Eqs. (2–4) and the selection of the ratios in Eq. (3) were determined by which value and ratio gave the smaller RMS value.

The calculated values are summarized in Table 2. In all cases, the RMS values of the CD spectra determined from the calculated values in Table 2 were slightly higher than the values obtained by the fitted curves shown in Figs. 4c–e and S2c. The comparison of the RMS values is made in Table S1 in the SI. Therefore, the calculated values give well-fitted CD spectra, as did the fitted curves using Eq. (1) (see Fig. S11 in the SI).

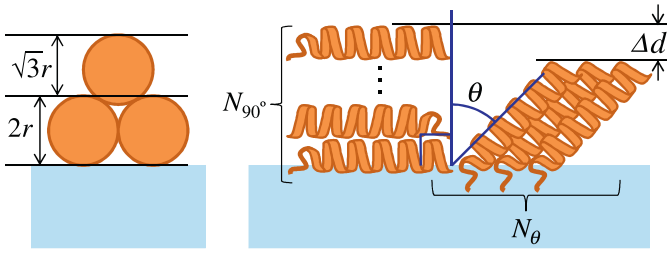

Fig. 11. Geometrical parameters for the structural model of the Langmuir monolayer under a surface pressure higher than that observed at the plateau of the isotherm.

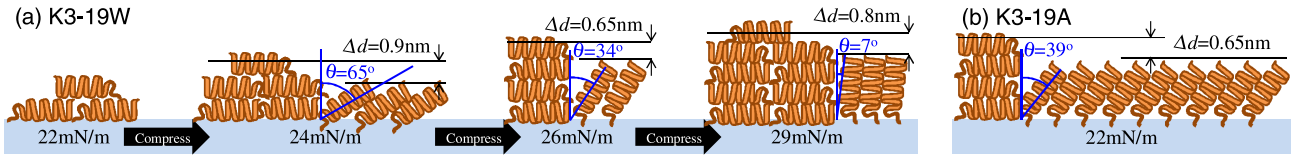

Fig. 12. Structure models of the helical AP monolayers of (a) K3-19W and (b) K3-19A on the subphase at 41.5 °C.

These calculations revealed that the high height regions in the AFM images (Figs. 8b, 9a, b, and 10c) consisted of horizontally aligned and overlapping helices for both peptides. In the case of K3-19W, as the surface pressure increased, both the fraction of the high height area $A_H/(A_H + A_L)$ and N_{90° increased but N_θ remained almost constant. Therefore, even when the subphase temperature was 41.5 °C, the transformation mode from $\theta = 90^\circ$ to $\theta < 90^\circ$ could not dominate over the 3D growth mode that induces the overlapped helices. The changes in the alignment and the orientation of the helices of K3-19W upon compression at 41.5 °C are summarized in Fig. 12a. Compression of the Langmuir monolayer induces the 3D growth mode at low surface pressure (<10 mN/m) and no tilted helices are found up to 22 mN/m. When the surface pressure reaches the pressure where the plateau region of the isotherm is observed (24 mN/m), the transformation mode is triggered and the tilt angle of the non-overlapping helices becomes less than 90°. Further compression promotes the 3D growth mode as well as the reduction of the tilt angle, and the helices involved in the transformation mode align their helical axes almost perpendicular ($\theta = 7^\circ$) to the surface. In the case of the K3-19A helices (Fig. 12b), the value of N_θ at the pressure where the plateau region of the isotherm is observed (22 mN/m) is larger than the case of the K3-19W helices. This difference can be ascribed to the difference in the HM value (Fig. 1). Because K3-19A has a smaller HM value than K3-19W, the K3-19A helices horizontally oriented at the air–water interface are more easily able to rotate than the K3-19W helices. The ease of rotation of the helices may lead to destabilization of the helix orientation upon compression. Therefore, the transformation mode of the K3-19A helices is triggered at a lower surface pressure than the K3-19W helices, and the value of N_θ of the K3-19A helices is larger than the K3-19W helices.

Mechanical properties of the Langmuir monolayers can be assessed by their surface compressibility modulus (K_s). Basically, the higher the value of K_s, the tighter the lateral packing of molecules. K_s is defined as the reciprocal of compressibility (C_s) as follows [48]:

$$K_s = C_s^{-1} = -A\left(\frac{\partial \pi}{\partial A}\right)_T. \quad (6)$$

The K_s–π isotherms of the Langmuir monolayers were calculated from the π–A isotherms and are shown in Fig. 13. Below the surface pressures at the plateau regions in the π–A isotherms (24 and 20 mN/m for K3-19W and K3-19A, respectively), the maximum value of K_s of the Langmuir monolayer of K3-19W ($K_s = 38$ mN/m, Fig. 13) was smaller than that of K3-19A ($K_s = 50$ mN/m, Fig. 13), suggesting that the K3-19W helices overlapped easier than the K3-19A helices. This suggestion qualitatively supports our analysis that the fraction of N_{90° of the K3-19W helices is larger than that of the K3-19A helices (Table 2). Above the surface pressures at the plateau regions in the π–A isotherms, a reasonable correlation between θ and K_s was observed in the Langmuir monolayer of K3-19W (Fig. 13). Because the denser the lateral packing, the higher the value of K_s, the value of K_s must increase as the value of θ decreases, and such dependence was observed for the K3-19W helices, i.e., $\theta = 34^\circ$ (Table 2) and $K_s = 12$ mN/m (Fig. 13) at $\pi = 26$ mN/m were changed to $\theta = 7^\circ$ (Table 2) and $K_s = 28$ mN/m (Fig. 13) at $\pi = 29$ mN/m. Furthermore, when the values of θ were similar ($\theta = 34^\circ$ and 39° for the K3-19W and K3-19A helices, respectively as listed in Table 2), the values of K_s were similar ($K_s = 12$ and 16 mN/m in the Langmuir monolayers of K3-19W and K3-19A, respectively as shown in Fig. 13). This similarity between K3-19W and K3-19A should be observed, because both APs formed the same secondary structure as the CD spectra in Figs. 4 and S2 indicated. Thus, the results of the analysis based on our structural model do not contradict to the mechanical property of the Langmuir monolayers.

4. Conclusions

The influence of the subphase temperature on the orientation of amphiphilic helices at the air–water interface was investigated. We found that increasing the subphase temperature from 21.5 to 41.5 °C leads to a plateau region in the π–A isotherm and a change in the helix orientation coupled with the surface pressure at the plateau. Because the helices overlapped without changing their orientation from 90° upon compression at 21.5 °C, we conclude that not only the compression of the Langmuir monolayer but also the thermal energy is important to trigger the change in the orientation of the horizontally aligned helices. To explain the formation of two different height regions observed in the monolayers transferred on the mica substrates, the uniform orientation model is inappropriate and an alternative model is proposed, where helices with two different orientations separately occur at the air–water interface. By allocating horizontally oriented helices and helices with a tilt angle $\theta < 90^\circ$ to the two different height regions, reasonable values of the parameters in the proposed model were calculated and the CD spectra calculated using the calculated values were in good agreement with the observed parameters. Based on the proposed model, the structural change of the Langmuir monolayer consisting of amphiphilic helices upon compression was determined. According to this model, the overlapping of horizontally oriented helices and the reduction in the tilt angle simultaneously occurred at and above the surface pressure at the plateau region observed in the π–A isotherm.

Table 2
Conditions and calculated values of N_{90°, N_θ, and θ.

Peptide	π_{dep} [mN/m]	Δd [nm]	A_H:A_L	MA [nm^2/molecule]	Radius (r) [nm]	N_{90°	N_θ	θ [degree]
K3-19W	24	0.90[a]	52:48[a]	1.84	0.55	2.3	1.5	65
K3-19W	26	0.64	69:31	0.90	0.5	3.7	1.6	34
K3-19W	29	0.81	77:23	0.74	0.5	4.6	1.5	7
K3-19A	22	0.64	24:76	0.99	0.5	3.5	9.3	39

[a] The values were obtained from Fig. 8b (see also Fig. S6).

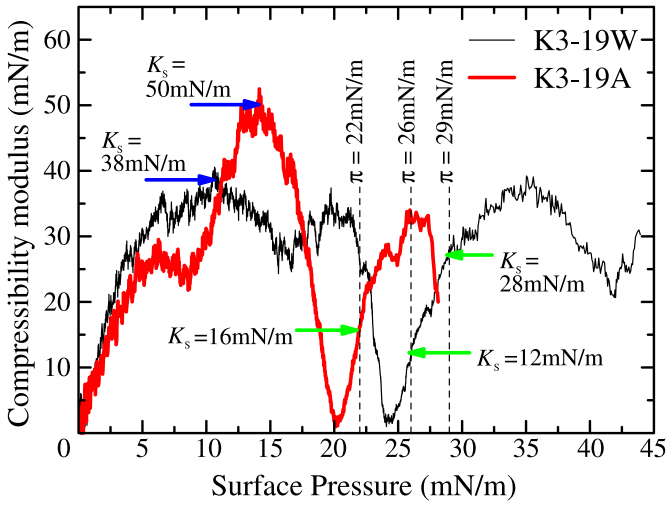

Fig. 13. K_s–π isotherms of the Langmuir monolayers of K3-19W (thin black line) and K3-19A (thick red line) at 41.5 ± 0.5 °C. Both were calculated from the π–*A* isotherms shown in Fig. 2b. Blue arrows indicate the maximum values of K_s below $\pi = 24$ and 20 mN/m for K3-19W and K3-19A, respectively. Green arrows indicate the values of K_s at $\pi = 26$ and 28 mN/m for K3-19W and that at $\pi = 22$ mN/m for K3-19A.

The influence of the HM value of the helix on the orientation of the amphiphilic helix at the air–water interface was also investigated. The hydrophobic domain of the K3-19W helix exhibits a larger HM value than that of the K3-19A helix. The Langmuir monolayer of K3-19A exhibited a plateau region in the π–*A* isotherm, which was coupled with the change in the helix orientation, at a lower surface pressure than that of K3-19W. The ratio of the number of tilted helices (N_θ) in the Langmuir monolayer of K3-19A was larger than that in the Langmuir monolayer of K3-19W, even though K3-19A exhibits a lower average hydrophobicity scale. Therefore, the hydrophobic domain of the amphiphilic helix should be designed to have a small HM value to allow the helix to more easily vertically orient at the interface.

Acknowledgements

Financial support from The Institute of Science and Technology, Meiji University is gratefully acknowledged. The authors also acknowledge significant experimental support from T. Iizuka, T. Dan, and T. Tanaka.

Appendix A. Supplementary data

Supplementary data to this article can be found online at http://dx.doi.org/10.1016/j.bbamem.2014.12.022.

References

[1] A.M. Seddon, P. Curnow, P.J. Booth, Biochim. Biophys. Acta 1666 (2004) 105.
[2] S.H. White, Protein Sci. 13 (2004) 1948.
[3] E. Wallin, G. von Heijne, Protein Sci. 7 (1998) 1029.
[4] M.S. Almén, K.J.V. Nordström, R. Fredriksson, H.B. Schiöth, BMC Biol. 7 (2009) 50.
[5] J.P. Overington, B. Al-Lazikani, A.L. Hopkins, Nat. Rev. Drug Discov. 5 (2006) 993.
[6] M.A. Yıldırım, K.-I. Goh, M.E. Cusick, A.-L. Barabási, M. Vidal, Nat. Biotechnol. 25 (2007) 1119.
[7] Membrane protein protocols: expression, purification, and characterization, in: B.S. Selinsky (Ed.), Methods in Molecular Biology, vol. 228, Humana Press Inc., New Jersey, 2003.
[8] Membrane Proteins, in: D.C. Rees (Ed.), Advances in Protein Chemistry, vol. 63, Academic Press, California, 2003.
[9] S.H. White, A.S. Ladokhin, S. Jayasinghe, K. Hristova, J. Biol. Chem. 276 (2001) 32395.
[10] A. Rath, D.V. Tulumello, C.M. Deber, Biochemistry 48 (2009) 3036.
[11] N. Bordag, S. Keller, Chem. Phys. Lipids 163 (2010) 1.
[12] H. Gillgren, A. Stenstam, M. Ardhammar, B. Nordén, E. Sparr, S. Ulvenlund, Langmuir 18 (2002) 462.
[13] M. Boncheva, H. Vogel, Biophys. J. 73 (1997) 1056.
[14] H. Yokoi, S. Hayashi, T. Kinoshita, Prog. Polym. Sci. 28 (2003) 341.
[15] D.W.P.M. Löwik, J.C.M. van Hest, Chem. Soc. Rev. 33 (2004) 234.
[16] A. Toyotama, S. Kugimiya, M. Yonese, T. Kinoshita, Y. Tsujita, Chem. Lett. (1997) 443.
[17] H. Hosolawa, T. Kinoshita, Y. Tsujita, H. Yoshimizu, Chem. Lett. (1997) 745.
[18] K. Kishihara, T. Kinoshita, T. Mori, Y. Okahata, Chem. Lett. (1998) 951.
[19] H. Yokoi, T. Kinoshita, Chem. Lett. 33 (2004) 426.
[20] S. Ye, J.W. Strzalka, B.M. Discher, D. Noy, S. Zheng, P.L. Dutton, J.K. Blasie, Langmuir 20 (2004) 5897.
[21] M. Merzlyakov, E. Li, K. Hristova, Langmuir 22 (2006) 1247.
[22] L.-T.T. Nguyen, A. Ardana, G. ten Brinke, A.J. Schouten, Langmuir 26 (2010) 6515.
[23] L.-T.T. Nguyen, A. Ardana, E.J. Vorenkamp, G. ten Brinke, A.J. Schouten, Soft Matter 6 (2010) 2774.
[24] L.-T.T. Nguyen, E.J. Vorenkamp, G. ten Brinke, A.J. Schouten, Langmuir 26 (2010) 11018.
[25] D. Jacquemain, S.G. Wolf, F. Leveiller, M. Deutsch, K. Kjaer, J. Als-Nielsen, M. Lahav, L. Leiserowitz, Angew. Chem. Int. Ed. Engl. 31 (1992) 130.
[26] P. Dutta, Colloids Surf., A 171 (2000) 59.
[27] Y.F. Yano, T. Uruga, H. Tanida, H. Toyokawa, Y. Terada, M. Takagaki, H. Yamada, Langmuir 25 (2009) 32.
[28] H. Tanida, Spectrochim. B 59 (2004) 1071.
[29] I. Cornut, B. Desbat, J.M. Turlet, J. Dufourcq, Biophys. J. 70 (1996) 305.
[30] A. Alessandrini, P. Facci, Meas. Sci. Technol. 16 (2005) R65.
[31] J. Meunier, Colloids Surf., A 171 (2000) 33.
[32] N. Kato, K. Saito, T. Serata, H. Aida, Y. Uesu, J. Chem. Phys. 115 (2001) 1473.
[33] M. Flörsheimer, D.H. Jundt, H. Looser, K. Sutter, M. Küpfer, P. Günter, Ber. Bunsenges. Phys.Chem. 98 (1994) 521.
[34] M. Flörsheimer, C. Birllert, H. Fuchs, Langmuir 15 (1999) 5437.
[35] A. Ulman, An Introduction to Ultrathin Organic Films: From Langmuir–Blodgett to Self-Assembly, Chap. 1 Academic Press Inc., California, 1991.
[36] K. Togashi, T. Iizuka, N. Kato, T. Sasaki, Y. Mukai, J. Nanosci. Nanotechol. 12 (2012) 568.
[37] K. Togashi, T. Iizuka, S. Yanagiya, N. Kato, T. Sasaki, Y. Mukai, e-J. Surf. Sci. Nanotech. 10 (2012) 379.
[38] L.-P. Liu, C.M. Deber, Biochemistry 36 (1997) 5476.
[39] Y. Yano, N. Shimai, K. Matsuzaki, J. Phys. Chem. B 114 (2010) 1925.
[40] D. Eisenberg, R.M. Weiss, T.C. Terwilliger, Proc. Natl. Acad. Sci. U. S. A. 81 (1984) 140.
[41] S.H. White, W.C. Wimley, Annu. Rev. Biophys. Biomol. Struct. 28 (1999) 319.
[42] A. Ulman, An Introduction to Ultrathin Organic Films: From Langmuir–Blodgett to Self-Assembly, Chap. 2.1 Academic Press Inc., California, 1991.
[43] Y. Wu, H.W. Huang, G.A. Olah, Biophys. J. 57 (1990) 797.
[44] I. Horcas, R. Fernandez, J.M. Gomez-Rodriguez, J. Colchero, J. Gomez-Herrero, A.M. Baro, Rev. Sci. Instrum. 78 (2007) 013705.
[45] G.A. Petsko, D. Ringe, Protein Structure and Function, Chap. 1 Oxford University Press, New York, 2009.
[46] Y. Yano, T. Takemoto, S. Kobayashi, H. Yasui, H. Sakurai, W. Ohashi, M. Niwa, S. Futaki, Y. Sugiura, K. Matsuzaki, Biochemistry 41 (2002) 3073.
[47] A. Ulman, An Introduction to Ultrathin Organic Films: From Langmuir–Blodgett to Self-Assembly, Chap. 2.9 Academic Press Inc, California, 1991.
[48] G.L. Gaines Jr., Insoluble Monolayers at Liquid–Gas Interfaces, Chap. 2, Sec. V Interscience Publishers, John Wiley & Sons, Inc., New York, 1966.